2-DOF Decoupled Discrete Current Control for AC Drives at Low Sampling-to-Fundamental Frequency Ratios

Meiqi Wang, *Member, IEEE*, Giampaolo Buticchi, *Senior Member, IEEE*, Jing Li, *Member, IEEE*, Chunyang Gu, *Member, IEEE*, David Gerada, *Senior Member, IEEE*, Michele Degano, *Senior Member, IEEE*, Lie Xu, *Member, IEEE*, Yongdong Li, *Senior Member, IEEE*, He Zhang, *Senior Member, IEEE, and* Chris Gerada, *Senior Member, IEEE*

***Abstract*—In high performance drive systems, wide bandwidth and reference tracking accuracy of current control loop are fundamental requirements. The conventional PI controller provides robustness against the machine parameter mismatching and zero steady-state error, but its dynamic performance degrades at high-speed due to the bandwidth limitation. In this paper, a new control structure of discrete PI controller with a deadbeat response is proposed, which combines the advantage of conventional PI controller with deadbeat characteristic. The proposed controller shows a decoupled tracking performance of up to 15% of the switching frequency, while also providing an extra control freedom of the disturbance rejection, which effectively improves the system stability. Experiments show a reduction of oscillation by 30% compared to the conventional PI and the validity and applicability of the proposed control method for high-speed applications with low sampling to fundamental frequency ratios.**

***Index Terms*—High speed AC drive, 2-DOF decoupled discrete PI (DDPI) design, decoupled current control, discrete-time system modeling, low S2F ratio.**

I. Introduction

In most high-performance industrial applications, such as in high-speed ac drive systems or medium voltage grid-connected converters, current control is a critical element, since its performance usually determines the overall system performance. A fast transient response and satisfactory steady state tracking performance is required [1].

During the past decades, remarkable efforts have been made in the development of high-performance current control, especially for ac machine drives. These include hysteresis regulator [2, 3], deadbeat controls [4-6], model predictive controls (MPC) [7-11], synchronous reference frame (SRF) proportional integral (PI) regulators and state feedback controls. Among them, the most widely used scheme is the PI current regulator, which has the advantage of robustness in cases of parameter mismatching and parameter variation due to saturation or temperature change [6, 12-14].

However, the bandwidth of a conventional PI regulator is limited by the time delay and discretization in digital implementation, which inhibits its use in high-performance drives [2, 13-16]. In high-speed applications, where a low ratio of sampling to fundamental (S2F) frequency is applied, high oscillation and even instability can occur if the design of the current regulator does not take these effects into account [14]. In transient states such as during sudden reference change and load disturbances, fast dynamic response is very important for high-speed drives. A slow transient characteristic not only degrades the performance of the current control but also causes further degradation of the outer speed control loop. Moreover, since conventional PI controllers are usually implemented in a synchronous reference frame (SRF), the cross-coupling of the states caused by the reference frame transformation deteriorates the dynamic performance of the current controller. Thus, although synchronous reference frame PI regulator provides the desirable performance in steady state, it is still of interest to improve its dynamic response.

Previous studies developed several control schemes for the digital inverter in order to improve the current regulating and dynamic performance and a summary is presented in TABLE I. For the digital implementation of continuous time domain design methods (i.e., SPI, FC-SPI and CPI), time delay compensation methods are suggested for further improving the dynamic response at low r_{S2F} [13, 15], and the active damping methods are introduced to improve the system disturbance rejection performance [17-21]. While the discrete time domain design methods provide a more straightforward way of decoupling design [14, 22-24], the proposal does not provide for full control of the closed-loop plant, which limits the controller capability in cases of disturbance rejection. Moreover, the constrained freedom of the control scheme restricts the ability of searching the optimal control voltage to force the current to the reference value in the minimum time possible, which causes a limited bandwidth and slower the dynamic response of the controller.

Manuscript received April 22, 2022; revised July 14, 2022 and September 01, 2022; accepted September 16, 2022. Date of publication; date of current version. This work is supported by Ningbo Science and Technology Bureau under S&T Innovation 2025 Major Special Programme with grant No. of 2019B10071. *(Corresponding author: Meiqi Wang).*

Meiqi Wang, David Gerada, Michele Degano and Chris Gerada are with Power Electronics and Machines and Control (PEMC) research group, University of Nottingham, Nottingham NG7 2RD, UK (e-mail: meiqi.wang1@nottingham.ac.uk; david.gerada@nottingham.ac.uk; michele.degano@nottingham.ac.uk; chris.gerada@nottingham.ac.uk)

Giampaolo Buticchi, Jing Li, Chunyang Gu, and He Zhang are with Power Electronics, Machines and Control (PEMC) research group, University of Nottingham Ningbo China, Ningbo 315104, China (e-mail: giampaolo.buticchi@nottingham.edu.cn; jing.li@nottingham.edu.cn; Chunyang.gu@nottingham.edu.cn; he.zhang@nottingham.edu.cn)

Lie Xu, Yongdong Li are with Electrical Engineering Department, Tsinghua University, Beijing 100190, China (e-mail: xulie@mail.tsinghua.edu.cn; liyd@mail.tsinghua.edu.cn)

Digital Object Identifier

TABLE I

Previous design methods of PI current regulator

Methods	Pro/Cons
SPI[17]	• Scalar-notation-based PI controller (SPI) [17], the most widely separated current control strategy due to simplicity to apply. • The current tracking performance is degraded by the cross-coupling effects due to digital implementation.
FC-SPI	• Feedforward compensated SPI Controller (FC-SPI), mathematically same as State feedback decoupling control methods. • Improved dynamic performance of SPI, However, performance degrades at low r_{S2F}.
IMC [18]	• Internal model control (IMC) provides adequate suppression of output disturbances. • However, the widely published IMC tuning rules, do a poor job suppressing load disturbances when the process dynamics are significantly slower than the desired closed-loop dynamics.
CPI [19-21]	• Complex-vector-based PI controller (CPI), provide a better decoupling performance and command tracking response than FC-SPI [12]. • Present a low capability of rejecting dc disturbance (with respect to stationary frame) in comparation of FC-SPI [19]
DPI [14, 22-24]	• Discrete time domain design method-based PI (DPI) controller, considering the effects of time delay and ZOH characteristic. Provide improved tracking performance at low r_{S2F} [14]. • Disturbance rejection performance is limited by the control freedom.

The cross-coupling effects in the current control system has been analyzed, and an accurate discrete-time-domain plant model has been developed in the previous work [25]. In this paper, a new control structure with both the satisfactory steady-state characteristics and fast transient response is proposed. The novelty of this paper lies in the design of the new structure of two degree of freedom (2-DOF) decoupled discrete PI (DDPI) control for low S2F ratios. Considering the discretization and time delay in digital control system, the controller is designed to eliminate the cross-coupling effects in synchronous reference frame (SRF) and ensure a decoupled tracking performance independent of the machine speed and S2F ratio. The proposed controller also features the deadbeat characteristic which provides a wide-bandwidth and low harmonic distortion solution for high-speed applications. This paper is organized as follows. In section II, an accurate system model considering the time delay and rotational transformation is built, and the cross-coupling in the current control system is analyzed. Section III analyzes the digital implementation and side effect of the existing design for low S2F applications, and subsequently an improved 2-DOF discrete PI controller is proposed. The latter is then verified by simulations and experiments, which are illustrated in section IV. To conclude, the matching results are shown in section V, where the benefits and applicability of the proposed decoupled discrete current control are highlighted.

II. Dynamic Model of PM Machine, Current Regulation and Back-EMF Decoupling

The nonlinear state equations governing the electrical and

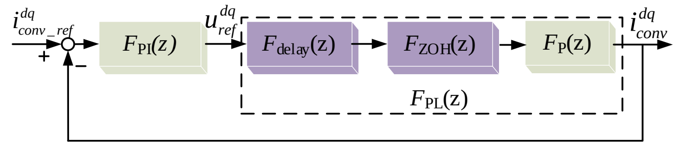

Fig 1. Simplified complex-frame control and plant model

electromagnetic behavior of a PM machine using complex vector notation, considering the armature voltage space vector $u^{\mathrm{dq}}_{\mathrm{Conv}}$ as the input, and armature current $i^{\mathrm{dq}}_{\mathrm{Conv}}$ as output variable of the motor, can be described by:

$$i^{\mathrm{dq}}_{\mathrm{Conv}} + \tau_\sigma \frac{\mathrm{d}}{\mathrm{d}\tau} i^{\mathrm{dq}}_{\mathrm{Conv}} = \frac{1}{r_\sigma} u^{\mathrm{dq}}_{\mathrm{Conv}} \underbrace{- j\omega_k L i^{dq}_{Conv} - j\omega_k \psi_f}_{cross-coupling} \quad (1)$$

ψ_{f} is space vector that represent the rotor flux linkage, τ_σ is the transient stator time constant, r_σ is the stator resistance, and ω_k is the electrical angular frequency. Ignoring the back-EMF influence and taking the electrical and electromagnetic behavior of a PM machine as well the sampling, calculation, and D/A transfer characteristics into account [14, 22], a simplified current transfer loop can be illustrated as shown in Fig. 1 with the complex-valued transfer function of system dynamic described in [25]:

$$F^{dq}_{PL}(s) = \frac{i^{dq}_{Conv}(s)}{u^{dq}_{ref}(s)}$$

$$= \underbrace{\frac{1-e^{-s\tau_s - j\omega_k\tau_s}}{s+j\omega_k}}_{ZOH} \underbrace{e^{-s\tau_d} e^{-j\omega_k\tau_d}}_{S\&C\ delay} \underbrace{\frac{1}{r_\sigma}\frac{1}{1+s\tau_\sigma + j\omega_k\tau_\sigma}}_{RL\ dynamic} \quad (2)$$

τ_{s} is the sampling period, τ_{d} is the time delay due to the sampling and calculating process. By introducing the transformation law to (2), the accurate discrete plant model considering the time delay and the transformation from stationary reference frame to rotational reference frame can be obtained:

$$F^{dq}_{PL}(z) = \frac{i^{dq}_{Conv}(z)}{u^{dq}_{ref}(z)} = \mathcal{Z}\left\{\mathcal{L}^{-1}\{F^{dq}_{PL}(s)\}\Big|_{t=k\tau_s}\right\} = \frac{K_s \cdot z^{-2}}{(1-\rho_2 z^{-1})} \quad (3)$$

It can be seen from (3), the plant model includes two poles in complex valued transfer function, the first pole $\rho_1 = 0$ is

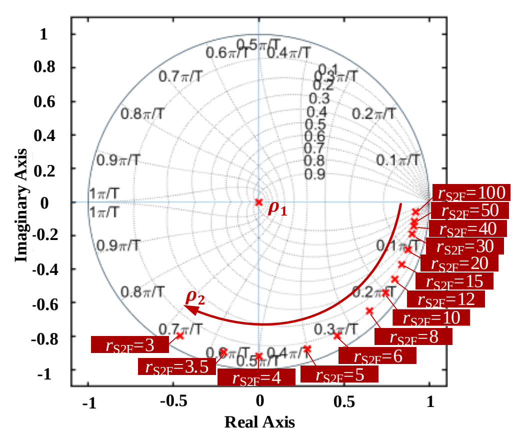

Fig. 2 Pole map of accurate plant model with varied r_{S2F}

located at origin and the second pole $\rho_2 = \delta_1\delta_2$ with $\delta_1 = e^{-\tau_s/\tau_\sigma}$, $\delta_2 = e^{-j\omega_k\tau_s}$, $K_s = \iota_1\iota_2$ is the system gain with $\iota_1 = (1-e^{-\tau_s/\tau_\sigma})/r_\sigma$, $\iota_2 = e^{-j2\omega_k\tau_s}$, $\mathcal{Z}$ and $\mathcal{L}^{-1}$represents the z-transformation and the inverse Laplace-transformation, respectively. The pole map of the accurate plant model in discrete time domain is illustrated in Fig. 2. As can be seen, the first pole ρ_1 is fixed to the coordinate origin of z-domain, while the second pole ρ_2 varies accordingly with the ratio of sampling to fundamental frequency ($r_{S2F} = f_s/f_e = \omega_s/\omega_k = 2\pi/\omega_k\tau_s$). As this ratio reduces, the system pole ρ_2 steps into the left half plane and the system gain K_s also changes.

III. Current Controller Design

A. Conventional PI current control

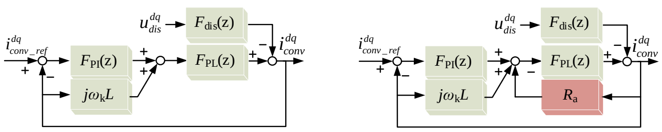

(a) FC-SPI (b) FC-SPI with active damping

Fig 3. Synchronous reference frame PI controllers

The schematic of the widely separated synchronous reference PI control with feedforward compensation decoupling method (hereinafter referred to as FC-SPI), is shown in Fig. 3(a). To improve the rejection of disturbance $u_{dis}^{dq}(s)$, in [26] it was suggested to implement an active resistance R_a in the digital controller, as shown in Fig. 3(b). This technique is named as 'active damping method', which has the same effect as increasing the resistance of the controlled machine, if the time delay and zero-order-hold characteristic are neglected [12].

However, the tracking performance and disturbance rejection performance of these controllers degrade at low S2F ratios where the practical issues caused by digital implementation process, such as inverter and sampling delay, cannot be ignored. As shown in Fig 4, the poles of the closed-loop system vary with S2F ratios, which indicate the incomplete decoupling and speed-dependent control performance.

B. Proposed 2-DOF DDPI

Due to the aforementioned limitations of conventional PI and active damping method in low S2F ratios, in this section, based on complex vector design method, a novel 2-DOF DDPI and its decoupling tuning method are proposed. The proposed method shows a frequency-independent dynamic response and improved stability. The scheme of proposed 2-DOF DDPI is shown in Fig. 5. A transfer function F_f^{dq} and a feedforward loop with an active damping gain K_{f3} is introduced to achieve the decoupling between the axes and the repositioning of the poles of plant (3).

$$F_f^{dq}(z) = \frac{K_{f1}}{1-K_{f2}\cdot z^{-1}} \tag{4}$$

Then the inner loop transfer function can be described as:

$$\frac{i_{Conv}^{dq}(z)}{u_{ref_1}^{dq}(z)} = \frac{K_{f1}K_s z^{-2}}{1-(K_{f2}+\rho_1)z^{-1}+(K_{f3}K_{f1}K_s+K_{f2}\rho_1)z^{-2}} \tag{5}$$

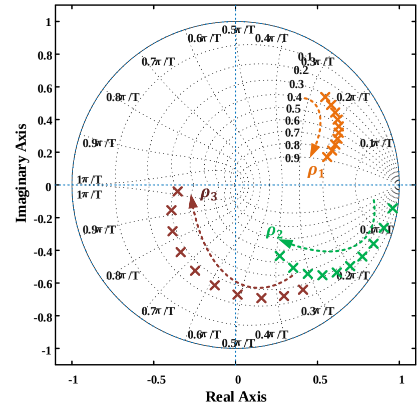

(a) reference

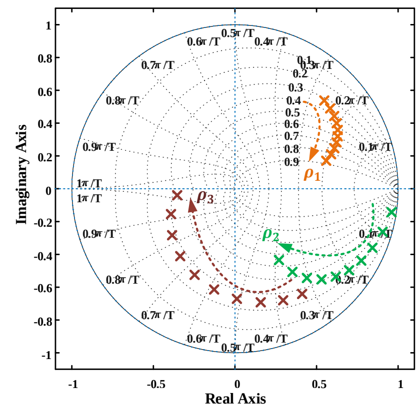

(b) disturbance

Fig. 4. Pole map of FC-SPI with active damping

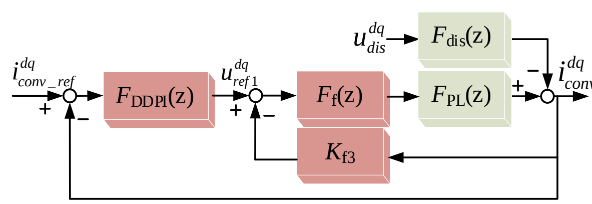

Fig. 5. 2-DOF discrete PI current controller

By properly choosing the values of gains K_{f1}, K_{f2}, and K_{f3}, the resulting system is completely decoupled, since all the coefficients involved in (5) are real numbers with:

$$K_{f1} = k_{c1}k_{c2} \tag{6}$$

$$K_{f2} = \rho_2 - \rho_1 \tag{7}$$

$$K_{f3} = -K_{f2}\rho_1 \tag{8}$$

$\rho_2 \in \mathrm{R}$, $|\rho_2| < 1$ is the constant parameter of the controller, which is selected by the designer. With this choice, the closed loop of the inner plant system results:

$$F_{C\_inner}^{dq}(z) = \frac{i_{Conv}^{dq}(z)}{u_{ref\_1}^{dq}(z)} = \frac{z^{-2}}{1-\rho_2 z^{-1}} \tag{9}$$

The poles are relocated to coordinate origin and ρ_2 along the real axis in the z plane as shown in Fig. 6. Comparing to (3) and Fig. 2, the poles of the revised inner loop do not change with different values of the mechanical angular velocity ω_k. This verifies that the internal loop is capable of decoupling axes *d*

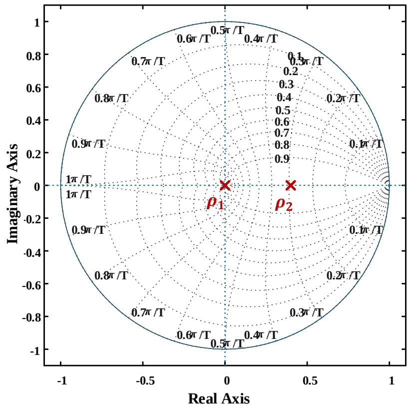

Fig. 6. Pole map of revised inner loop.

and q and relocating the poles. The outer-loop of DDPI controller (10) is designed to regulate the current tracking performance, with the zero z_0 used to compensate the pole ρ_2 of $F_{C\_\text{inner}}^{dq}(z)$, with controller gain K_c equal to the real-valued factor γ, $\gamma > 0$ is introduced to shape the command response of the current controller, where $\gamma \in R$ is a constant.

$$F_{DDPI}^{dq}(z) = \frac{u_{ref\_1}^{dq}(z)}{i_{Conv\_ref}^{dq}(z) - i_{Conv}^{dq}(z)} = K_c \frac{1 - z_0 z^{-1}}{1 - z^{-1}} \tag{10}$$

$$z_0 = \rho_2 \tag{11}$$

$$K_c = \gamma \tag{12}$$

The closed-loop transfer function of the system without disturbance results:

$$F_{C\_ref}^{dq}(z) = \frac{i_{Conv}^{dq}(z)}{i_{Conv\_ref}^{dq}(z)} = \frac{\gamma z^{-2}}{1 - z^{-1} + \gamma z^{-2}} \tag{13}$$

While considering the disturbance in the control system, the closed-loop transfer function of system is obtained:

$$i_{Conv}^{dq}(z) = \gamma \frac{z^{-2}}{1 - z^{-1} + \gamma z^{-2}} i_{Conv_{ref}}^{dq}(z) + \underbrace{\frac{z^{-2}}{1 - z^{-1} + \gamma z^{-2}}}_{F_{dis\_A}^{dq}(z)} \cdot \underbrace{\frac{\iota_1 \iota_2 (1 - z^{-1})(1 - K_{f2} z^{-1})}{z^{-1} \cdot (1 - \rho_2 z^{-1})}}_{F_{dis\_B}^{dq}(z)} \cdot u_{dis}^{dq}(z) \tag{14}$$

It can be noticed that the disturbance transfer function $F_{dis\_B}^{dq}(z)$ in (14) has the pole located at ρ_2 which is a constant tuning parameter chosen by designers and does not change with the rotating frequency ω_k. Designers can use the real-valued factor γ to shape the command response of the current controller and use ρ_2 to improve the disturbance rejection dynamics and system stability, as illustrated in Fig. 7.

C. PDPI (High-bandwidth tuning methods of 2-DOF DDPI)

In this section, the predictive decoupled PI (PDPI) controller is proposed, featuring the same structure but with different tuning method compared to that presented earlier in section B. It presents the deadbeat characteristic, provides high bandwidth, and further improves the dynamic response. The conventional PI controllers have limited bandwidth because there is only one degree of freedom (1-DOF) and, as a result, this scheme cannot find the optimal control voltage which will force the current to

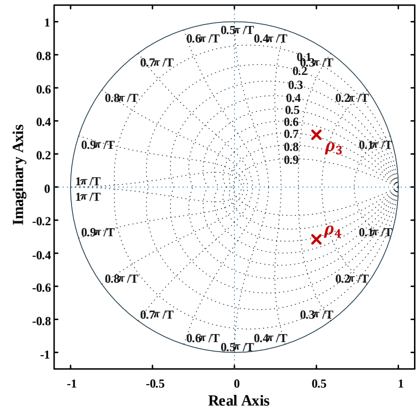

(a) reference

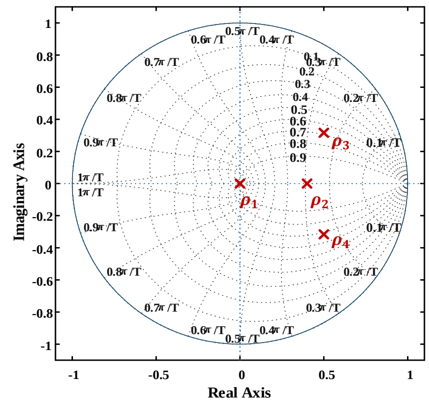

(b) disturbance

Fig. 7. Pole map of 2-DOF DDPI at varied S2F ratios.

the reference value in the minimum possible time. By changing the tuning method of 2-DOF DDPI, a wide bandwidth solution with deadbeat characteristic can be achieved with:

$$K_{f1} = k_{c1} k_{c2} \tag{15}$$

$$K_{f2} = \rho_3 + \rho_2 - \rho_1 \tag{16}$$

$$K_{f3} = \rho_2 \rho_3 - K_{f2} \rho_1 \tag{17}$$

The inner loop transfer function is then obtained as:

$$F_{C\_\text{inner}}^{dq}(z) = \frac{i_{Conv}^{dq}(z)}{u_{ref\_1}^{dq}(z)} = \frac{z^{-2}}{(1 - \rho_2 z^{-1})(1 - \rho_3 z^{-1})} \tag{18}$$

By employing $z_0 = \rho_2, K_c = 1$ to (10) and $\rho_3 = -1$ to (18), the closed-loop transfer function of the system is obtained:

$$F_{C\_ref}^{dq}(z) = \frac{i_{Conv}^{dq}(z)}{i_{Conv\_ref}^{dq}(z)} = \frac{K_c z^{-2}}{1 - \underbrace{(\rho_3 + 1)}_{\zeta_1} z^{-1} + \underbrace{(K_c + \rho_3)}_{\zeta_2} z^{-2}} = z^{-2} \tag{19}$$

It can be seen from (19) that the transfer function shows a deadbeat characteristic, which allows for a fast-tracking performance. Considering the disturbance in the control system, the closed-loop transfer function of system is obtained:

$$i_{Conv}^{dq}(z) = z^{-2} \cdot i_{Conv_{ref}}^{dq}(z) + \underbrace{z^{-2}}_{F_{dis\_A}^{dq}(z)} \cdot \underbrace{\frac{\iota_1 \iota_2 (1 - z^{-1})(1 - K_{f2} z^{-1})}{z^{-1} \cdot (1 - \rho_2 z^{-1})}}_{F_{dis\_B}^{dq}(z)} \cdot u_{dis}^{dq}(z) \tag{20}$$

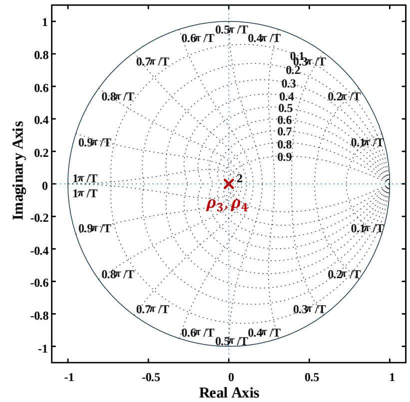

(a) reference

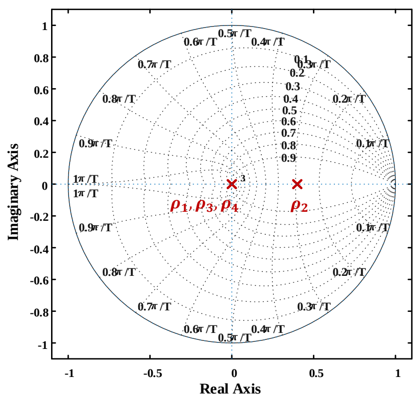

(b) disturbance

Fig. 8. Pole map of PDPI at varied S2F ratios.

Comparing the closed loop pole maps Fig.7 and Fig.8 with Fig.4, it can be seen, the proposed 2-DOF DDPI controllers present a S2F ratio-independent characteristic. Additionally, it provides an adjusted disturbance rejection ability without affecting controller tracking performance.

IV. Analysis and Verification

A. Simulation and experimental setup.

To verify the proposed 2-DOF DDPI current regulator, simulations are performed within MATLAB/Simulink environment, where a continuous time-domain PMSM model (parameters obtained from experimental test results), an average model of two-level inverter (with one-step delay of output voltage) and a discrete controller are used. The inductance values of test machine are shown in Fig 9, and the other parameters are shown in Table Ⅱ.

The validation of the proposed control strategy is also performed on a 120 krpm high speed dynamometer with the SiC inverter-fed high speed SPM prototype, as shown in Fig. 10. The SiC based two-level inverter is designed for high-speed application, where the maximum switching frequency is equal to 80kHz, and the dead time is equal to 500 ns. During the tests, the switching frequency is set as 10 kHz to emphasize control performances with reduced samples per fundamental period. The controllers for the experimental tests are implemented on the designed DSP + FPGA controller board. During the experimental test, the dyno works in speed mode and the test motor works in load mode to validate the proposed current

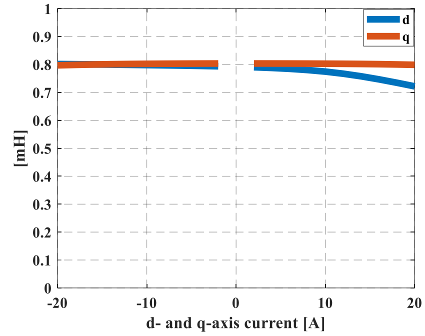

Fig 9. Machine inductance corresponding to different current.

TABLE II
Test Machine Parameters

Parameter	Value	Units
Rated power	5	kW
Rated speed	80k	rpm
Phase resistance	0.67	Ω
Pole pairs	2	

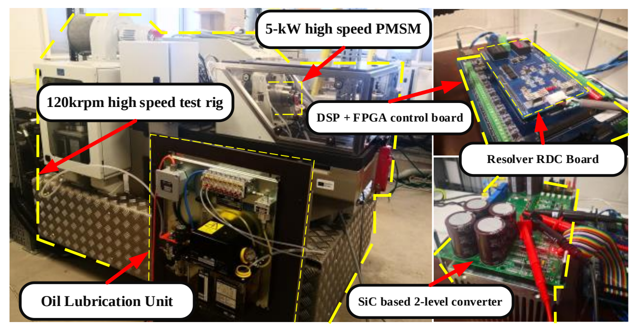

Fig 10. Experimental test platform.

control strategy. The same PWM frequency and control frequency are used in all simulations and experiments presented in this paper.

B. Performance Analysis of Proposed DDPI

1). Simulation results: Firstly, the dynamic response of conventional PI controller (FC-SPI) and proposed 2-DOF DDPI controllers are compared in simulation.

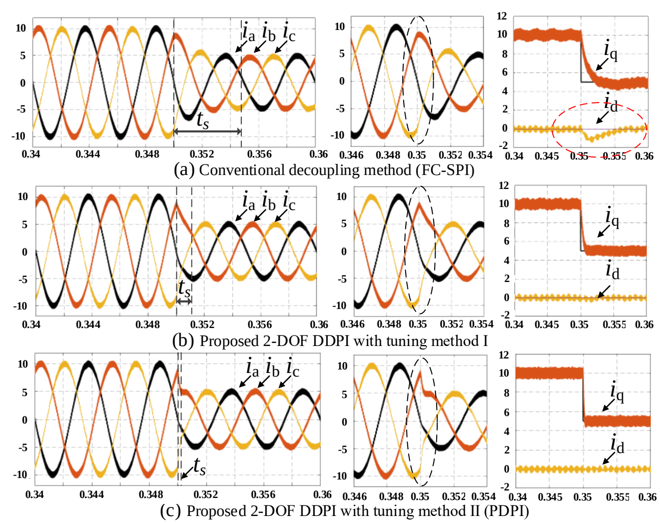

(a) Conventional decoupling method (FC-SPI)

(b) Proposed 2-DOF DDPI with tuning method I

(c) Proposed 2-DOF DDPI with tuning method II (PDPI)

Fig 11. Transient response at 6000rpm, ratio = 50.

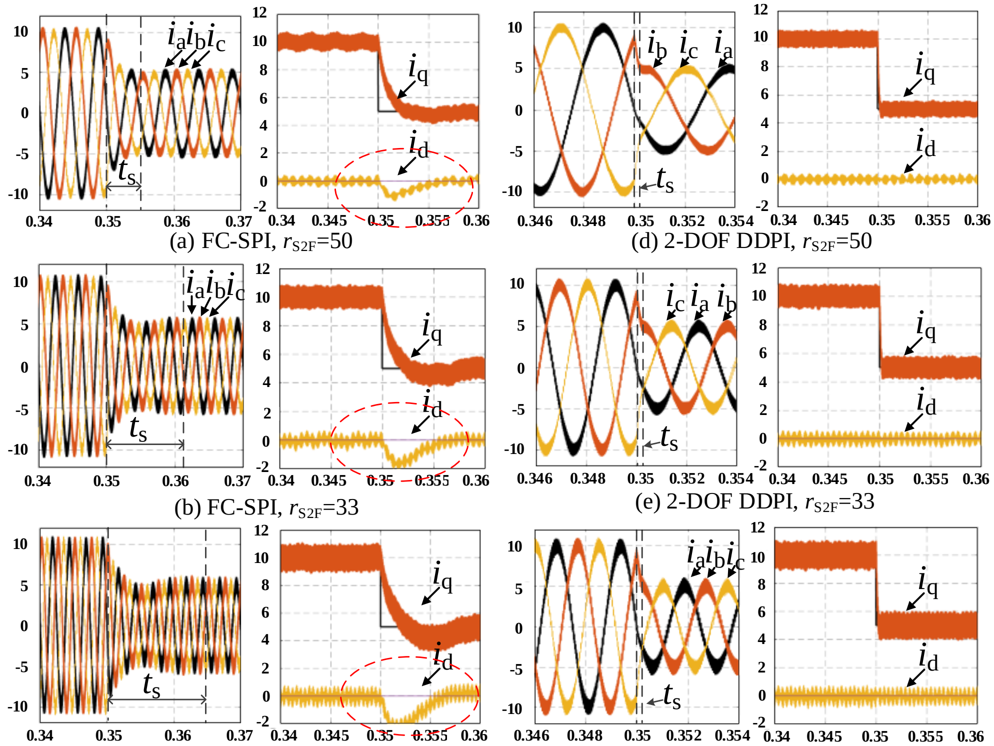

(a) FC-SPI, r_{S2F}=50 (d) 2-DOF DDPI, r_{S2F}=50

(b) FC-SPI, r_{S2F}=33 (e) 2-DOF DDPI, r_{S2F}=33

(c) FC-SPI, r_{S2F}=25 (f) 2-DOF DDPI, r_{S2F}=25

Fig. 12. Transient response comparison between FC-SPI (left) and proposed PDPI (right) with varied S2F ratios.

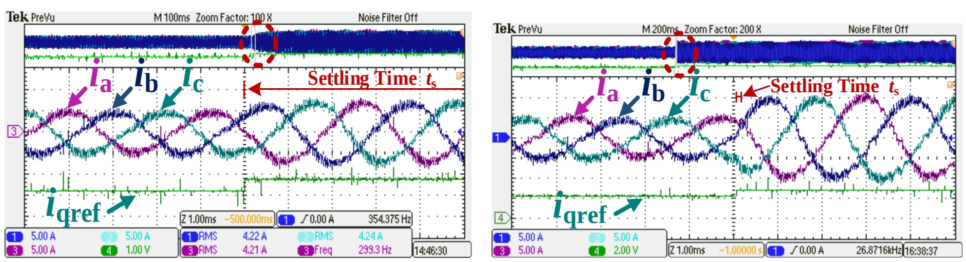

(a) FC-SPI. (b) 2-DOF DDPI (PDPI)

Fig. 13. Dynamic responses comparison at 9krpm, ratio = 33.

Fig. 11 presents the transient response of different regulators at high sampling to fundamental frequency ratio, i.e., r_{S2F} = 50. From top to bottom, Fig. 11(a) presents the performance of conventional decoupling method FC-SPI, which shows the longest settling time (t_s = 50T_s) and around 10% overshoot of d-axis current (which indicate the incomplete decoupling). The performance of the proposed 2-DOF DDPI shows a fast-tracking performance (t_s = 10T_s) and zero overshoot of i_d (Fig. 11(b)). Additionally, with the proposed predictive tuning method, 2-DOF DDPI presents decoupled control performance with the deadbeat characteristic, which tracks the reference value in two steps (t_s = 2T_s), as shown in Fig.11(c). The decoupling performance of proposed 2-DOF DDPI with decreased S2F ratios is tested, as shown in Fig. 12. It can be seen from (a) to (c), as S2F ratio decreases, conventional decoupling method FC-SPI shows a degrading tracking performance with increased setting time (from 50T_s to 150T_s) and overshoot of d-axis current (from 10% to 22%). On the other hand, the proposed 2-DOF DDPI shows S2F ratio-independent dynamic response and tracks the reference value in 2T_s, as shown in Fig 12 (d) to (f). It is also worth mentioning that at extreme low S2F ratio, i.e., below 10, control system with FC-SPI becomes unstable, while the proposed 2-DOF DDPI can keep the same decoupled deadbeat control performance as shown in Fig 12.

2). Improved dynamic performance and decoupled control at different frequency/ratios: The decoupled control performance and the high bandwidth characteristic of proposed 2-DOF DDPI have been verified in the experimental test. Firstly, the tracking performances of FC-SPI and the proposed controller have been compared at relatively high S2F ratio (r_{S2F}=33), as shown in Fig. 13. The settling time (t_s) are marked, and the transient behavior of each method is highlighted by the red dash circle in the figure. It can be seen from Fig. 13(a), during the sudden load change, the conventional PI presents a slow tracking performance (t_s> 50T_s). While the proposed 2-DOF DDPI presents high bandwidth characteristic which tracks the reference value in two steps (t_s = 2T_s), shown in Fig. 13(b). The decoupled control performance of proposed 2-DOF DDPI controller with varied S2F ratios has been verified both in d-q domain and a-b-c domain, as shown in Fig. 14 and Fig. 15-17. In Fig. 14(a), the

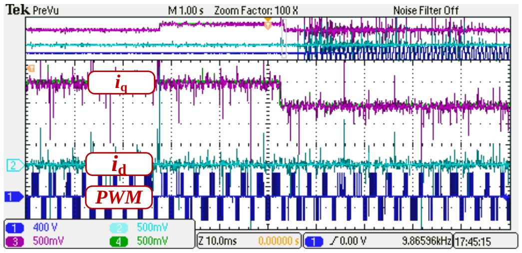

(a) 9000 rpm, ratio = 33 and f_e = 300Hz

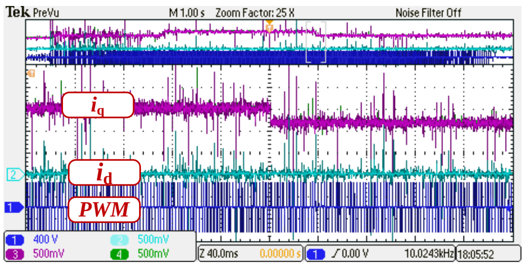

(b) 12000 rpm, ratio = 25 and f_e = 400Hz

Fig. 14. Dynamic responses of proposed PDPI with sudden q-axis current reference change.

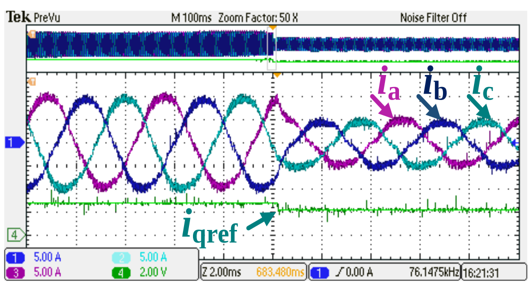

Fig. 15. Transient responses of PDPI at 6krpm, ratio = 50.

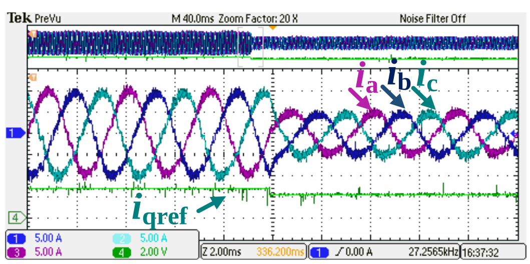

Fig. 16. Transient responses of PDPI at 9krpm, ratio = 33.

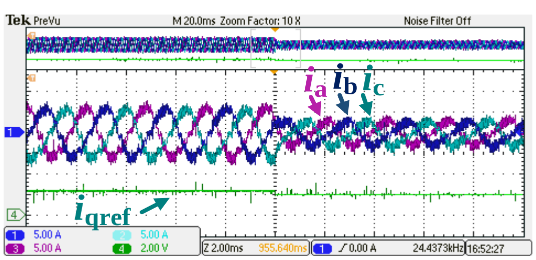

Fig. 17. Transient responses of PDPI at 12krpm, ratio = 25.

dynamic response of proposed control with a q-axis current reference step change (10A to 5A) at 9000 rpm is presented. It can be seen there is no cross-coupling between *d* and *q* axes currents, and the controller present a fast-tracking performance

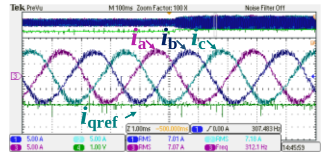

(a) FC-SPI

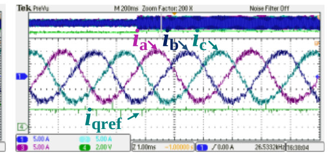

(b) 2-DOF DDPI (PDPI).

Fig. 18. Steady-state responses at 9krpm, ratio = 33.

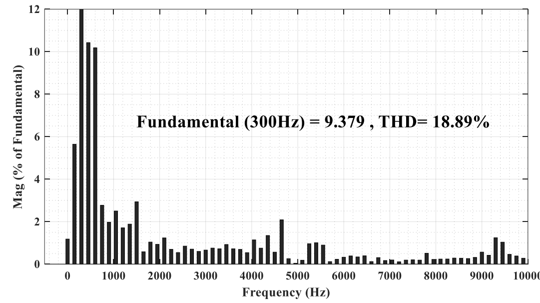

(a) FC-SPI

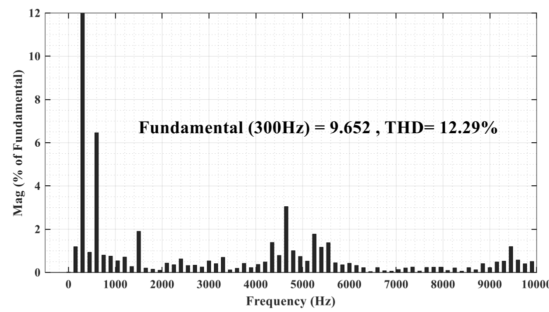

(b) 2-DOF DDPI (PDPI)

Fig. 19. THD% of phase current at 9krpm, ratio = 33

without overshoot, this matches with the simulation results shown in Fig. 12(e). Same decoupled control performance at low S2F ratio (r_{S2F} = 25) is illustrated in Fig.14 (b), which experimentally verified the simulation results shown in Fig. 12(f).

The S2F ratio-independent decoupled tracking performance with minimum settling time of the proposed 2-DOF DDPI has been verified at stationary reference domain. The three-phase currents tracking performance with different S2F ratios, during sudden change of load, are shown in Fig. 15 to Fig. 17. The S2F ratio is reduced as the speed increase, but the current control settling time keep the same. The proposed controller presents a high bandwidth characteristic which tracks the reference value in two steps (t_s = 2T_s) regardless of the S2F ratio. The same conclusion can be also drawn from Fig. 12 (d) to (f).

3). Improved steady-state performance and THD%: The steady-state performance is compared and shown in Fig. 18. This experimental benchmark has confirmed the effectiveness of the proposed 2-DOF DDPI controller over the PI controller in terms of an overall low THD. The harmonic mitigation capability of the proposed DDPI controller and the PI controller is compared, as shown in Fig.19 and 20.

As shown in Fig. 19, the PI controller can maintain lower harmonics in a wide range of frequencies (e.g., 4kHz). The low frequency harmonics close to the fundamental frequency are reduced (Fig. 20) and the fundamental component increases by

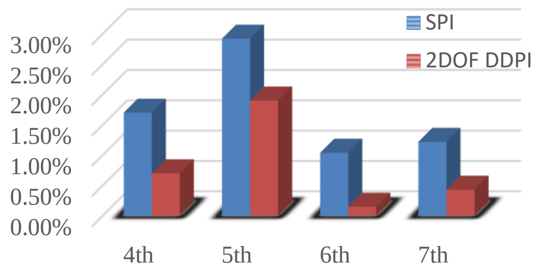

Fig. 20. Low-order harmonics component amplitudes comparison between FC-SPI and 2-DOF DDPI (PDPI).

2.91%, while the total THD% is reduced by 30% with respect to the conventional PI controller (Fig. 19). These results are confirming the benefits of the method introduced and its applicability to high-speed drives where the sampling to fundamental frequency ratios is low.

4). Performance under parameter mismatching: The effect of the parameter variation on the controllers has been analysis using simulation, for two different tunings methods, as shown in Fig. 21 and 22. Here L is the machine real inductance value and L' is the machine parameter used in the control. It can be noticed that both tuning methods keep the same tracking performance with fixed settling time, the decoupled control performance is not affected by the parameter mismatch.

V. Conclusion

In this paper, a novel 2-DOF decoupled discrete PI method is proposed, which aims to eliminate the cross-coupling between d- and q- axes, and improves the dynamic response of conventional PI controllers. The proposed 2-DOF scheme provides an extra control freedom of the disturbance rejection, which effectively improves the system stability without effecting the tracking performance.

Furthermore, two decoupled tuning methods for the proposed 2-DOF DDPI have been designed. One is for decoupled control with improved stability, while the other is for decoupled control with deadbeat characteristics.

The proposed method is performed experimentally on a 5 kW high-speed SPMSM, with the matching simulation and practical test results validating the theoretical analysis. Without current and flux observers, the proposed discrete-time domain current controller allows to guarantee decoupled tracking performance of up to 15% of the switching frequency with respect to the state-of-art discrete current control of 8.3% [14]. The total THD% is reduced by a significant 30% compared to the conventional controller.

Appendix

The tuning method of conventional PI controller used in the paper has been explained in detail in the previous work [25]. To realize the maximum bandwidth, $k_{max} \approx \frac{9.3}{100} \cdot 2\pi f_s$ is selected as the controller gain in this paper. The discretization process of the conventional controller is illustrated as follow.

Synchronous PI (SPI) controller in s-domain:

$$F_{SPI}^{dq}(s) = k_c \frac{(\tau_i s+1)}{\tau_i s} = \frac{k r_\sigma (1+s\tau_\sigma)}{s} \quad (21)$$

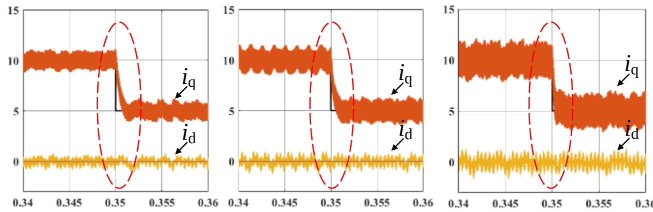

(a) $L = 1.3L'$ (b) $L = L'$ (c) $L = 0.7L'$

Fig. 21. 2-DOF DDPI (method I) at 12000 rpm, $r_{S2F} = 25$

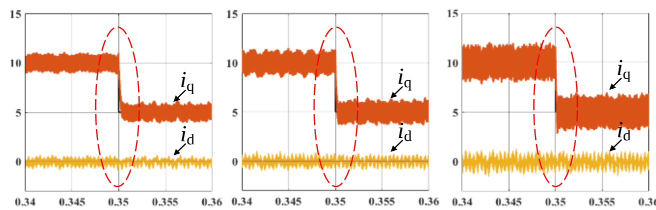

(a) $L = 1.3L'$ (b) $L = L'$ (c) $L = 0.7L'$

Fig. 22. 2-DOF DDPI (PDPI) at 12000 rpm, $r_{S2F} = 25$

By combining with the current feedback with gain $j\omega_k L_\sigma$ added at the output of $F_{SPI}(s)$, the imaginary part of the plant pole in $F_P^{dq}(s)$ can be canceled, i.e., it replaces the plant transfer function by $F_P^{dq}(s - j\omega_k) = 1/r_\sigma(1+s\tau_\sigma)$, which is used in Feedforward Compensated SPI (FC-SPI). The resulting pole of $F_P^{dq}(s - j\omega_k)$ is compensated by the zero of controller (21), and the open loop transfer function of the current control system can be presented as:

$$F_O^{dq}(s) = F_{SPI}^{dq}(s) \cdot F_P^{dq}(s - j\omega_k) = \frac{k}{s} \quad (22)$$

Considering the time delay and the characteristic of D/A, and using the Tustin transformation, the PI current controller in the discrete time domain can be described as (23),

$$F_{SPI}^{dq}(z) = F_{SPI}^{dq}(s)\Big|_{s=\frac{2}{\tau_s}\frac{z-1}{z+1}} = A \cdot \frac{1}{1-z^{-1}} + B \cdot \frac{z^{-1}}{1-z^{-1}} \quad (23)$$

Where $A = k_c\left(1+\frac{1}{2}\tau_s\tau_i^{-1}\right)$, $B = k_c(\frac{1}{2}\tau_s\tau_i^{-1} - 1)$, and the close-loop transfer function being (24):

$$F_C^{dq}(z) = \frac{u_{ref}^{dq}(z)}{i_{Conv_{ref}}^{dq}(z)} = \frac{AK_s \cdot z^{-2} + BK_s z^{-3}}{1-(1+\rho_1)z^{-1}+(AK_s+\rho_1)z^{-2}+BK_s z^{-3}} \quad (24)$$

Acknowledgment

This work is supported by Ningbo Science and Technology Bureau under S&T Innovation 2025 Major Special Programme with grant No. of 2019B10071.

References

[1] C. Jong-Woo and S. Seung-Ki, "Fast current controller in three-phase AC/DC boost converter using d-q axis crosscoupling," *IEEE Transactions on Power Electronics*, vol. 13, no. 1, pp. 179-185, 1998, doi: 10.1109/63.654973.

[2] D. G. Holmes, B. P. McGrath, and S. G. Parker, "Current Regulation Strategies for Vector-Controlled Induction Motor Drives," *IEEE Transactions on Industrial Electronics*, vol. 59, no. 10, pp. 3680-3689, 2012, doi: 10.1109/tie.2011.2165455.

[3] R. Ramchand, K. Gopakumar, C. Patel, K. Sivakumar, A. Das, and H. Abu-Rub, "Online Computation of Hysteresis Boundary for Constant Switching Frequency Current-Error Space-Vector-Based Hysteresis Controller for VSI-Fed IM Drives," *IEEE Transactions*

on Power Electronics, vol. 27, no. 3, pp. 1521-1529, 2012, doi: 10.1109/TPEL.2011.2120624.
[4] L. Springob and J. Holtz, "High-bandwidth current control for torque-ripple compensation in PM synchronous machines," *IEEE Transactions on Industrial Electronics,* vol. 45, no. 5, pp. 713-721, 1998, doi: 10.1109/41.720327.
[5] J. Holtz and L. Springob, "Identification and compensation of torque ripple in high-precision permanent magnet motor drives," *IEEE Transactions on Industrial Electronics,* vol. 43, no. 2, pp. 309-320, 1996, doi: 10.1109/41.491355.
[6] M. Tang, A. Gaeta, K. Ohyama, P. Zanchehtta, and G. Asher, "Assessments of dead beat current control for high speed permanent magnet synchronous motor drives," in *2015 9th International Conference on Power Electronics and ECCE Asia (ICPE-ECCE Asia)*, 1-5 June 2015 2015, pp. 1867-1874, doi: 10.1109/ICPE.2015.7168033.
[7] J. Rodriguez *et al.*, "Predictive Current Control of a Voltage Source Inverter," *IEEE Transactions on Industrial Electronics,* vol. 54, no. 1, pp. 495-503, 2007, doi: 10.1109/TIE.2006.888802.
[8] S. Kouro, P. Cortes, R. Vargas, U. Ammann, and J. Rodriguez, "Model Predictive Control—A Simple and Powerful Method to Control Power Converters," *IEEE Transactions on Industrial Electronics,* vol. 56, no. 6, pp. 1826-1838, 2009, doi: 10.1109/TIE.2008.2008349.
[9] J. Rodriguez *et al.*, "State of the Art of Finite Control Set Model Predictive Control in Power Electronics," *IEEE Transactions on Industrial Informatics,* vol. 9, no. 2, pp. 1003-1016, 2013, doi: 10.1109/TII.2012.2221469.
[10] X. Sun, T. Li, Z. Zhu, G. Lei, Y. Guo, and J. Zhu, "Speed Sensorless Model Predictive Current Control Based on Finite Position Set for PMSHM Drives," *IEEE Transactions on Transportation Electrification,* vol. 7, no. 4, pp. 2743-2752, 2021, doi: 10.1109/TTE.2021.3081436.
[11] Q. Wang *et al.*, "A Low-Complexity Optimal Switching Time-Modulated Model-Predictive Control for PMSM With Three-Level NPC Converter," *IEEE Transactions on Transportation Electrification,* vol. 6, no. 3, pp. 1188-1198, 2020, doi: 10.1109/TTE.2020.3012352.
[12] A. G. Yepes, A. Vidal, J. Malvar, O. Lopez, and J. Doval-Gandoy, "Tuning Method Aimed at Optimized Settling Time and Overshoot for Synchronous Proportional-Integral Current Control in Electric Machines," *IEEE Transactions on Power Electronics,* vol. 29, no. 6, pp. 3041-3054, 2014, doi: 10.1109/tpel.2013.2276059.
[13] B. Bon-Ho and S. Seung-Ki, "A compensation method for time delay of full-digital synchronous frame current regulator of PWM AC drives," *IEEE Transactions on Industry Applications,* vol. 39, no. 3, pp. 802-810, 2003, doi: 10.1109/TIA.2003.810660.
[14] K. Hongrae, M. W. Degner, J. M. Guerrero, F. Briz, and R. D. Lorenz, "Discrete-Time Current Regulator Design for AC Machine Drives," *IEEE Transactions on Industry Applications,* vol. 46, no. 4, pp. 1425-1435, 2010, doi: 10.1109/tia.2010.2049628.
[15] M. Lu, X. Wang, P. C. Loh, F. Blaabjerg, and T. Dragicevic, "Graphical Evaluation of Time-Delay Compensation Techniques for Digitally Controlled Converters," *IEEE Transactions on Power Electronics,* vol. 33, no. 3, pp. 2601-2614, 2018, doi: 10.1109/TPEL.2017.2691062.
[16] D. G. Holmes, T. A. Lipo, B. P. McGrath, and W. Y. Kong, "Optimized Design of Stationary Frame Three Phase AC Current Regulators," *IEEE Transactions on Power Electronics,* vol. 24, no. 11, pp. 2417-2426, 2009, doi: 10.1109/tpel.2009.2029548.
[17] A. Petersson, L. Harnefors, and T. Thiringer, "Evaluation of current control methods for wind turbines using doubly-fed induction machines," *IEEE Transactions on Power Electronics,* vol. 20, no. 1, pp. 227-235, 2005, doi: 10.1109/TPEL.2004.839785.
[18] J. Yim, S. Sul, B. Bae, N. R. Patel, and S. Hiti, "Modified Current Control Schemes for High-Performance Permanent-Magnet AC Drives With Low Sampling to Operating Frequency Ratio," *IEEE Transactions on Industry Applications,* vol. 45, no. 2, pp. 763-771, 2009, doi: 10.1109/TIA.2009.2013600.
[19] L. Harnefors, K. Pietilainen, and L. Gertmar, "Torque-maximizing field-weakening control: design, analysis, and parameter selection," *IEEE Transactions on Industrial Electronics,* vol. 48, no. 1, pp. 161-168, 2001, doi: 10.1109/41.904576.
[20] H. A. Hussain, "Tuning and Performance Evaluation of 2DOF PI Current Controllers for PMSM Drives," *IEEE Transactions on Transportation Electrification,* vol. 7, no. 3, pp. 1401-1414, 2021, doi: 10.1109/TTE.2020.3043853.
[21] A. M. Diab, S. Bozhko, M. Galea, and C. Gerada, "Stable and Robust Design of Active Disturbance-Rejection Current Controller for Permanent Magnet Machines in Transportation Systems," *IEEE Transactions on Transportation Electrification,* vol. 6, no. 4, pp. 1421-1433, 2020, doi: 10.1109/TTE.2020.3001042.
[22] N. Hoffmann, F. W. Fuchs, M. P. Kazmierkowski, and D. Schroder, "Digital current control in a rotating reference frame - Part I: System modeling and the discrete time-domain current controller with improved decoupling capabilities," *IEEE Transactions on Power Electronics,* vol. 31, no. 7, pp. 5290-5305, 2016, doi: 10.1109/tpel.2015.2481726.
[23] A. Altomare, A. Guagnano, F. Cupertino, and D. Naso, "Discrete-Time Control of High-Speed Salient Machines," *IEEE Transactions on Industry Applications,* vol. 52, no. 1, pp. 293-301, 2016, doi: 10.1109/tia.2015.2478750.
[24] K. Huh and R. D. Lorenz, "Discrete-Time Domain Modeling and Design for AC Machine Current Regulation," in *2007 IEEE Industry Applications Annual Meeting*, 23-27 Sept. 2007 2007, pp. 2066-2073, doi: 10.1109/07IAS.2007.312.
[25] M. Wang *et al.*, "Decoupled Discrete Current Control for AC Drives at Low Sampling-to-Fundamental Frequency Ratios," *IEEE Journal of Emerging and Selected Topics in Power Electronics,* pp. 1-1, 2022, doi: 10.1109/JESTPE.2022.3179184.
[26] F. B. d. Blanco, M. W. Degner, and R. D. Lorenz, "Dynamic analysis of current regulators for AC motors using complex vectors," *IEEE Transactions on Industry Applications,* vol. 35, no. 6, pp. 1424-1432, 1999, doi: 10.1109/28.806058.

Meiqi Wang (Member, IEEE) received the B.Eng. degree in electrical engineering from the Northeast Electric Power University, Jilin, China, in 2014. During 2014 to 2017, she was a joint training master student in electrical engineering of Tsinghua University, Beijing, and Northeast Electric Power University, Jilin, China. She is currently pursuing the Ph.D. degree with the Power Electronics, Machines and Control (PEMC) Group, University of Nottingham, Nottingham, U.K.

Her research interests include power electronics and advanced control techniques for high-speed permanent magnet machines and synchronous reluctance machines for transportation electrification.

Giampaolo Buticchi (Senior Member, IEEE) received the master's degree in electronic engineering and the Ph.D. degree in information technologies from the University of Parma, Parma, Italy, in 2009 and 2013, respectively. In 2012, he was a Visiting Researcher with the University of Nottingham, Nottingham, U.K. Between 2014 and 2017, he was a Postdoctoral Researcher and Von Humboldt Postdoctoral Fellow with the University of Kiel, Kiel, Germany. In 2017, he was appointed as an Associate Professor in Electrical Engineering with the University of Nottingham Ningbo China, Ningbo, China, and as a Head of Power Electronics of the Nottingham Electrification Centre. He was promoted to Professor in 2020.

His research focuses on power electronics for renewable energy systems, smart transformer fed microgrids and dc grids for the More Electric Aircraft. He is one of the advocates for dc distribution systems and multiport power electronics onboard the future aircraft. He is author/co-author of more than 230 scientific papers. Dr. Buticchi is currently the Chair of the IEEE-IES Technical Committee on Renewable Energy Systems and the IES Energy Cluster Delegate. During his stay in Germany, he was awarded with the Von Humboldt Postdoctoral Fellowship to carry out research related to fault tolerant topologies of smart transformers. He is an Associate Editor for the IEEE TRANSACTIONS ON INDUSTRIAL ELECTRONICS, the IEEE TRANSACTIONS ON TRANSPORTATION ELECTRIFICATION, and the IEEE Open Journal of the Industrial Electronics Society.

Jing Li (Member, IEEE) received the B.Eng. and M.Sc. degrees (Hons.) from the Beijing Institute of Technology, Beijing, China, in 1999 and 2002, respectively, and the Ph.D. degree from the University of Nottingham, Nottingham, U.K., in 2010, all in electrical and electronic engineering. She was a Research Fellow after graduation with the Power Electronic, Machine and Control Group, University of Nottingham. In 2016, she joined the University of Nottingham Ningbo China, Ningbo, China, as an Assistant Professor, where she is currently an Associate Professor with the Department of Electrical and Electronic Engineering.

Her research interests include condition monitoring for motor drive systems and power distribution systems, advanced control, and design of motor drive systems.

Chunyang Gu (Member, IEEE) received the B.Sc. degree in electrical engineering from the Harbin Institute of Technology, Harbin, China, in 2010, and the Ph.D. degree in electrical engineering from Tsinghua University, Beijing, China, in 2015. In 2015, she went to the University of Nottingham, U.K., where she was a Postdoctoral Research Fellow with the Power Electronics, Machines and Control (PEMC) Research Group. Since 2017, she has been an Assistant Professor with the Department of Electrical and Electronic Engineering and the PEMC Research Group, University of Nottingham Ningbo China, Ningbo, China.

Her research interests include power electronics for transportation electrification, renewable energy and grid applications, e.g., solid-state transformer, solid-state circuit breaker, multilevel converter topologies and control, application of wide-bandgap semiconductor devices, power electronics in EV, railway, marine, and MEA.

David Gerada (Senior Member, IEEE) received the Ph.D. degree in high-speed electrical machines from the University of Nottingham, Nottingham, U.K., in 2012. From 2007 to 2016, he was with the Research and Development Department, Cummins, Stamford, U.K., first as an Electromagnetic Design Engineer from 2007 to 2012, and then as a Senior Electromagnetic Design Engineer and Innovation Leader from 2012 to 2016. At Cummins, he pioneered the design and development of high-speed electrical machines, transforming a challenging technology into a reliable one suitable for the transportation market, while establishing industry-wide-used metrics for such machinery. In 2016, he joined the University of Nottingham, where he is currently a Principal Research Fellow in electrical machines, responsible for developing state-of-the-art electrical machines for future transportation that push existing technology boundaries while propelling the new technologies to higher technology readiness levels.

Dr. Gerada is a Chartered Engineer in the U.K. and a member of the Institution of Engineering and Technology.

Michele Degano (Senior Member, IEEE) received the master's degree in electrical engineering from the University of Trieste, Trieste, Italy, in 2011, and the Ph.D. degree in industrial engineering from the University of Padova, Padova, Italy, in 2015. From 2014 to 2016, he was a Postdoctoral Researcher with The University of Nottingham, Nottingham, U.K., where he joined the Power Electronics, Machines and Control (PEMC) Research Group. In 2016, he joined the University of Nottingham as an Assistant Professor in Advanced Electrical Machines and appointed as an Associate Professor in 2020 and as a Professor in 2022. He is currently the PEMC Director of Industrial Liaison leading research projects for the development of future hybrid electric aerospace platforms and electric transports.

His main research interests include electrical machines and drives for industrial, automotive, railway, and aerospace applications, ranging from small to large power.

Lie Xu (Member, IEEE) was born in Beijing, China, in 1980. He received the B.S. degree in electrical and electronic engineering from the Beijing University of Aeronautics and Astronautics, Beijing, China, in 2003, and the M.S. and Ph.D. degrees in electrical and electronic engineering from The University of Nottingham, Nottingham, U.K., in 2004 and 2008, respectively. From 2008 to 2010, he was a Research Fellow with the Department of Electrical and Electronic Engineering, The University of Nottingham. He is currently an Associate Professor with the Department of Electrical Engineering, Tsinghua University, Beijing, China.

His research interests include multilevel converters, direct ac–ac power conversion, and multilevel matrix converters.

Yongdong Li (Senior Member, IEEE) was born in Hebei, China, in 1962. He received the B.S. degree in electrical engineering from the Harbin Institute of Technology, Harbin, China, in 1982, and the M.S. and Ph.D. degrees in electrical engineering from the Department of Electrical Engineering, Institute National Polytechnique de Toulouse, Toulouse, France, in 1984 and 1987, respectively. Since 1996, he has been a Professor with the Department of Electrical Engineering, Tsinghua University, Beijing, China.

His research interests include power electronics, machine control, and transportation electrification.

He Zhang (Senior Member, IEEE) received the B.Eng. degree from Zhejiang University, Hangzhou, China, in 2002, and the M.Sc. and Ph.D. degrees in electrical machines from the University of Nottingham, Nottingham, U.K., in 2004 and 2009, respectively. He was a Research Fellow with the University of Nottingham and the Director of the BestMotion Technology Centre. He moved to the University of Nottingham Ningbo China, Ningbo, China, as a Senior Research Fellow in 2014 and a Principal Research Fellow in 2016. He is currently the Director of the Nottingham Electrification Centre, Power Electronics, Machines and Control Research Group, University of Nottingham.

His research interests include high-performance electric machines and drives for transport electrification.

Chris Gerada (Senior Member, IEEE) received the Ph.D. degree in numerical modelling of electrical machines from the University of Nottingham, Nottingham, U.K., in 2005. He was a Researcher with the University of Nottingham on high-performance electrical drives and on the design and modelling of electromagnetic actuators for aerospace applications. In 2008, he was appointed as a Lecturer in electrical machines; in 2011, as an Associate Professor; and in 2013, as a Professor with the University of Nottingham. He is currently an Associate Pro-Vice-Chancellor for industrial strategy and impact and a Professor of electrical machines with the University of Nottingham. He has authored or co-authored more than 350 referred publications.

His principal research interest includes electromagnetic energy conversion in electrical machines and drives, focusing mainly on transport electrification. He has secured over £20 M of funding through major industrial, European, and U.K. grants. Dr. Gerada was the Research Chair of the Royal Academy of Engineering in 2013 and also the Chair of the IEEE IES Electrical Machines Committee. He was an Associate Editor of the IEEE TRANSACTIONS ON INDUSTRY APPLICATIONS.